

# On the mechanical behaviour of PEEK and HA cranial implants under impact loading



D. Garcia-Gonzalez<sup>a</sup>, J. Jayamohan<sup>b</sup>, S.N. Sotiropoulos<sup>c</sup>, S.-H. Yoon<sup>d</sup>, J. Cook<sup>d</sup>, C.R. Siviour<sup>d</sup>, A. Arias<sup>a</sup>, A. Jérusalem<sup>d,\*</sup>

<sup>a</sup> Department of Continuum Mechanics and Structural Analysis, University Carlos III of Madrid, Avda. de la Universidad 30, 28911 Leganés, Madrid, Spain

<sup>b</sup> Department of Neurosurgery, John Radcliffe Hospital, Oxford University Hospitals, Oxford OX3 9DU, UK

<sup>c</sup> Oxford Centre for Functional Magnetic Resonance Imaging of the Brain, John Radcliffe Hospital, Oxford OX3 9DU, UK

<sup>d</sup> Department of Engineering Science, University of Oxford, Parks Road, Oxford OX1 3PJ, UK

## ARTICLE INFO

### Keywords:

Finite element head model

Cranial implant

PEEK

Macroporous HA

Impact loading

## ABSTRACT

The human head can be subjected to numerous impact loadings such as those produced by a fall or during sport activities. These accidents can result in skull fracture and in some complex cases, part of the skull may need to be replaced by a biomedical implant. Even when the skull is not damaged, such accidents can result in brain swelling treated by decompressive craniectomy. Usually, after recovery, the part of the skull that has been removed is replaced by a prosthesis. In such situations, a computational tool able to analyse the choice of prosthesis material depending on the patient's specific activity has the potential to be extremely useful for clinicians. The work proposed here focusses on the development and use of a numerical model for the analysis of cranial implants under impact conditions. In particular, two main biomaterials commonly employed for this kind of prosthesis are polyether-ether-ketone (PEEK) and macroporous hydroxyapatite (HA). In order to study the suitability of these implants, a finite element head model comprising scalp, skull, cerebral falx, cerebrospinal fluid and brain tissues, with a cranial implant replacing part of the skull has been developed from magnetic resonance imaging data. The human tissues and these two biocompatible materials have been independently studied and their constitutive models are provided here. A computational model of the human head under impact loading is then implemented and validated, and a numerical comparison of the mechanical impact response of PEEK and HA implants is presented. This comparison was carried out in terms of the effectiveness of both implants in ensuring structural integrity and preventing traumatic brain injury. The results obtained in this work highlight the need to take into account environmental mechanical considerations to select the optimal implant depending on the specific patient: whereas HA implants present attractive biointegration properties, PEEK implant can potentially be a much more appropriate choice in a demanding mechanical life style. Finally, a novel methodology is proposed to assess the need for further clinical evaluation in case of impact with both implants over a large range of impact conditions.

## 1. Introduction

The human head is often subjected to impact loading during automobile accidents, falls or sport-related events. These impact conditions can lead to mechanically-induced head injury, which constitutes one of the major causes of accidental death (Sahoo et al., 2016). Head injuries are generally grouped into three categories: scalp damage, skull fracture, brain injury, or a combination of these (Khalil and Hubbard, 1977). Skull fracture occurs when the tolerance limit of the skull is exceeded due to mechanical loading. These fractures result in permanent damage and account for 32% of all head injuries

sustained by pedestrians, motorcyclists, vehicle occupants and sportsmen (Fredriksson et al., 2001). In some cases, where there is contamination from a laceration, the fractured zone of the skull can be removed and later replaced by a biomedical implant whose main functions are cosmetic and to act as a structural component protecting the brain against external loads. However, the replacement of part of the skull does not necessarily result from skull fracture. In this regard, cranial implants are also widely used after decompressive craniectomy. This has become a relatively common intervention when managing traumatic brain injury (TBI), subarachnoid hemorrhage, severe intracranial infection and stroke (Honeybul and Ho, 2016). In these terms,

\* Corresponding author.

E-mail address: [antoine.jerusalem@eng.ox.ac.uk](mailto:antoine.jerusalem@eng.ox.ac.uk) (A. Jérusalem).

the main aim of neurosurgeons dealing with the reconstruction of large and complex-formed bone defects is a predictable and stable functional and aesthetic result (Eolchiyan, 2014). Often, when decompressive surgery is needed, the use of an autologous bone for large cranial reconstructions is not possible due to size, unacceptable appearance, or infection, fragmentation and bone resorption after grafting (Rosenthal et al., 2014). Neurosurgeons have to choose a material to be used; polyether-ether-ketone (PEEK) and macroporous hydroxyapatite (HA) are the most common biomaterials selected due to their biocompatibility and mechanical properties.

PEEK is a semi-crystalline thermoplastic polymer considered as an engineering material for use in high-quality applications due to its excellent mechanical and thermal properties as well as good chemical resistance (Garcia-Gonzalez et al., 2015a, 2015b). Large cranial defects are often dealt with through cranioplasties involving PEEK implants designed from preoperative high-resolution computed tomography (CT) scans. The direct contact between the implant and bone tissue is ensured by the customisation of the implant from the CT images thus achieving a precise definition of its contour and curvature (El Halabi et al., 2011). The suitability of using PEEK for implants is known and its biocompatibility has been studied and demonstrated (Horak et al., 2010; Jockisch et al., 1992; Rivard et al., 2002).

Macroporous HA is a bioceramic material which constitutes 60% of bone, and has similar mechanical characteristics. This material exhibits a number of properties which make it suitable to be used in skull defect reconstructions: biocompatible, sterilisable, adequate weight, compatible with diagnostic imaging and easy to design and manufacture (Stefini et al., 2013). The presence of calcium and phosphate ions (similarly to natural bone) participates to the formation of new bone tissues on the surface of the implant (Chistolini et al., 1999). Furthermore, HA mimics the macroporous structure of the living bone. This structure allows new bone to grow by filling not only the voids on the surface of the cranioplasty, but also the pores within the internal structure (Frassanito et al., 2013). As such, once the prosthesis has been placed in the skull and bone has grown within, the implant can be treated as a composite material where HA acts as the matrix and bone as the reinforcement. Moreover, HA shows excellent biocompatibility due to the absence of host immune reactions (Boyde et al., 1999; Maracci et al., 1999; Olmi et al., 1984). However, despite these advantages, HA implants are rigid and offer a considerably lower resilience than human bone. This fact implies a minor mechanical resistance and minor energy absorption capability with respect to human bone (Frassanito et al., 2013).

When dealing with large cranial defects, an important aspect to take into account is the load-bearing capacity of the structural prostheses, since the patients need to go back to active life, with their heads potentially subjected to future impact loadings. While the use of biocompatible materials such as PEEK and HA in cranial implants is widely accepted, there is a lack of knowledge in terms of their mechanical response under potential future impact loads arising from the patient life style. The main aim of the research presented in the current paper is to develop a computational tool able to simulate the mechanical behaviour of implants under impact loading which can help clinicians to determine the optimal patient-specific implant material. As a second contribution, a numerical tool is proposed to evaluate the risk of implant failure when a patient has been involved in a given accidental impact. To this end, a finite element head model (FEHM) has been developed from magnetic resonance imaging (MRI) data comprising scalp, skull, cerebral falx, cerebrospinal fluid (CSF), brain tissues and an implant replacing part of the skull. The constitutive models of the human tissues included in the FEHM are individually chosen from the literature. For the PEEK, a constitutive model previously developed and validated for this specific material by the authors is used (Garcia-Gonzalez et al., 2017). An experimental programme aimed at characterising experimentally macroporous HA has been carried out with specimens manufactured from a real cranial

implant. As a second step, its mechanical properties after bone regrowth have been numerically estimated. The FEHM is then used to study the mechanical response under a wide range of impact conditions. Numerical simulations were conducted in order to compare the mechanical response of PEEK and HA cranial implants. This analysis was carried out by focussing on the implant effectiveness in avoiding failure and TBI, while covering an impact velocity range from 1 m/s to 7 m/s for several impact locations on the skull along three different paths: from the parietal zone to vertex; from the parietal zone to occipital; and from the parietal zone to frontal. Ultimately, selection criteria for implant materials and a roadmap for further clinical assessments of bone and/or implant failure in case of post-operative impact are proposed.

2. Materials and methods

This section introduces the methodology followed in the development of the numerical head model for impact loading. Special attention is first paid to the mechanical characterisation of each human tissue and the correct identification of the boundary conditions during the impact process. The FEHM is then presented.

2.1. Mechanical behaviour of human head tissues and biomaterials

In this section, the constitutive modelling of each tissue and biomaterial is discussed in detail.

2.1.1. Scalp

Ottenio et al. (2015) tested skin specimens from a human back and identified an anisotropic rate-dependent behaviour of the skin. These properties are known to vary with its localisation in the human body as has been observed in experimental studies (Annaiidha et al., 2012; Dunn and Silver, 1983; Khatam et al., 2014; Jacquemoud et al., 2007; Vogel, 1972; Zahouani et al., 2009).

More particularly, Gambarotta et al. (2005) carried out an experimental and numerical study of the mechanical behaviour of human scalp. The authors finally proposed a rate-independent, isotropic and hyperelastic constitutive model based on the phenomenological scheme developed by Tong and Fung (1976). However, because of the computational cost of numerical simulations which involve a full head model, most previous FEHM traditionally define scalp as an isotropic and homogeneous material through linear elastic constitutive laws (Horgan and Gilchrist, 2003; Liu et al., 2007; Sahoo et al., 2014; Willinger et al., 2000; Zhang et al., 2001). In this work, the scalp mechanical behaviour has thus been assumed to be rate-independent, isotropic, homogeneous and linear elastic, see Table 1. Note that, when a cranial implant is needed, the mechanical properties of this tissue can vary both in time and space in the zone affected by the surgery. While fully integrated HA could potentially be considered to be surrounded by the same surrounding tissue mechanical properties as in a normal situation (with full skull), such argumentation is not straightforwardly justifiable in the case of PEEK. However, as the immediate surrounding tissue (damaged or not) is in any case much softer than either the implants or the bone, it most likely does not influence significantly the

Table 1  
Material properties for scalp.

Scalp			
Density (kg/m <sup>3</sup> )	Poisson's ratio	Young's modulus (MPa)	Reference
1100	0.42	16.7	(Horgan and Gilchrist, 2003; Liu et al., 2007; Sahoo et al., 2014 Zhang et al., 2001)

**Table 2**  
Material properties for skull bone and falx.

Tissue	Density (kg/m <sup>3</sup> )	Poisson's ratio	Young's modulus (MPa)	Reference
Skull bone	1728	0.22	8000	(Wood, 1971)
Falx	1133	0.45	31.5	(Chafi et al., 2010; Takhounts et al., 2008)

different failure modes. Additionally, it must be emphasised that we do not consider any postoperative complication that can arise from the implant integration (or lack thereof). Therefore, we assume herein that a potential difference in the mechanical response of scalp can be neglected with respect to the overall response of the head-structure, thus defining the same material properties for both cases when the cranial implant is considered and otherwise.

### 2.1.2. Skull and falx

The bone microstructure is a complex, heterogeneous, multiphasic and anisotropic composite (Doblaré et al., 2004; Tse et al., 2015). However, most of the FEHM published before have constitutively defined the skull bone behaviour as isotropic, homogeneous and linear elastic as a first approximation (El Halabi et al., 2011; Sahoo et al., 2014; Takhounts et al., 2008; Tse et al., 2015; Willinger et al., 1995; Zhang et al., 2001). In this work, following the material description assumed by these authors, the skull bone structure is treated as an isotropic, homogeneous and linear elastic material. However, since skull bone is composed by two external layers of cortical bone and a core of cancellous bone, a homogenised Young's modulus has been defined based on the modulus of each layer and their thicknesses, see Table 2. The mechanical properties for cortical bone are based on the experimental data reported by Wood (1971), where the data defining the Young's modulus (GPa) of the cranial human bone for different strain rates was fitted as:

$$E = 16 + 1.93 \log(\dot{\epsilon}) \quad (1)$$

where  $E$  is the Young Modulus and  $\dot{\epsilon}$  the strain rate.

The mechanical properties of cancellous bone core, also known as diploe, can be obtained from the experimental work published by Melvin et al. (1969). Both cortical and cancellous bones' Young's moduli were selected for a strain rate of  $1 \text{ s}^{-1}$ , the average strain rate observed on the skull structure in the numerical simulations of this work.

The falx cerebri is a layer of the dura mater located between the cerebral hemispheres which plays an important role in restricting brain motion. Here, it is geometrically defined as isolated from the dura mater and in direct contact with bone. The constitutive behaviour of the falx is defined as linear elastic (Chafi et al., 2010; Kleiven et al., 2002; Takhounts et al., 2008; Zhou et al., 1995), see Table 2.

### 2.1.3. Mechanical behaviour of CSF and ventricles

CSF is a biological fluid with Newtonian characteristics that fills the space between the skull and the brain tissues, as well as the ventricles (Ommaya, 1968). Under impact conditions, the CSF plays a protective role by damping brain movement and reducing shear stresses. In previous works where a FEHM has been used, some authors described the CSF mechanical behaviour as linear elastic (Gao, 2007; Giovanni et al., 2005; Horgan and Gilchrist, 2003; Horgan and Gilchrist, 2004; Sahoo et al., 2014; Zhang et al., 2001). However, due to the Newtonian behaviour of the CSF and its similarity with water in terms of viscosity (Horgan and Gilchrist, 2004; Ommaya, 1968), a more accurate description of the CSF viscous constitutive behaviour is adopted here with the mechanical properties of water:

**Table 3**  
Material properties for CSF.

CSF and ventricles					
Density (kg/ m <sup>3</sup> )	$c_0$ (m/s)	$s$	$\Gamma_0$	$\eta$ (Pa s)	Reference
1000	1450	1.99	0.11	0.00089	(Jérusalem and Dao, 2012)

$$\sigma = -PI + 2\eta\dot{\epsilon}' \quad (2)$$

where  $P$  is the pressure,  $\mathbf{I}$  is the identity tensor,  $\eta$  is the dynamic viscosity and  $\dot{\epsilon}'$  is the deviatoric strain rate. The viscosity of the material drives the shear stress contribution while the pressure  $P$  corresponds to the volumetric stress contribution. Under shock conditions,  $P$  depends on the current density  $\rho$  through the Mie-Grüneisen equation of state:

$$P = \frac{\rho_0 c_0^2 \zeta}{(1 - s\zeta)^2} \left( 1 - \frac{\Gamma_0 \zeta}{2} \right) + \Gamma_0 \rho_0 E_m \quad (3)$$

where  $\zeta = 1 - \rho_0/\rho$  is the nominal volumetric compressive strain with  $\rho_0$  as the initial density,  $c_0$  is the speed of sound in water,  $s$  is the slope of the  $u_s$ – $u_p$  curve in the Hugoniot formulation, where  $u_s$  and  $u_p$  are the shock and particle velocities.  $\Gamma_0$  is the Grüneisen coefficient and  $E_m$  is the internal energy per unit mass. The values of the material parameters for CSF are given in Table 3.

The ventricles being filled with CSF are assumed here to have CSF mechanical properties (Zhang et al., 2001).

### 2.1.4. Brain tissue

Human brain tissue as a whole has been defined as a nonlinear solid with very small volumetric drained compressibility and viscous contributions to its solid phase deformation (Goriely et al., 2015). In this work, the human brain was separated into gray and white matters. This division allows for a more accurate determination of the brain injuries induced by the impact loading. Some authors, who have considered the brain tissue as a whole, describe the brain mechanical behaviour as linear elastic (Khalil and Hubbard, 1977; Liu et al., 2007; Ruan et al., 1991; Shuck and Advani, 1972; Ueno et al., 1989; Willinger et al., 1999; Willinger et al., 2000). Other authors include a linear viscoelastic law with a relaxation shear modulus for the whole brain (Jirousek et al., 2005; Rashid et al., 2014; Sahoo et al., 2014; Tse et al., 2015; Willinger et al., 2000; Zhang et al., 2001). However, the distinction between gray and white matters is mechanically necessary, since white matter has been found to be stiffer than gray matter in compression and shear (Budday et al., 2015). The authors following this approach usually follow a linear viscoelastic law for the relaxation shear moduli (Al-Bsharat et al., 1999; Horgan and Gilchrist, 2004; Zhang et al., 2001). In addition, some authors introduced the anisotropy of white matter arising from the presence of axons in the description of the mechanical behaviour through an anisotropic visco-hyperelastic material law (Sahoo et al., 2014).

Because the type of impacts considered here is assumed to mostly affect the gray matter, one unique set of parameters is used for the mechanical behaviour of both gray and white matters. The value for the bulk modulus was determined experimentally by Stalnaker (1969). The effects of the brain viscoelasticity in shear behaviour are taken into account through the following expression:

$$G(t) = G_\infty + (G_0 - G_\infty)e^{-\beta t} \quad (4)$$

where  $G_0$ ,  $G_\infty$  and  $\beta$  represent the short-time modulus, the long-time modulus and the decay constant. Note that for simplicity, the expression is presented under a constant strain condition; its full formulation and implementation involved the usual convolution used in viscoelastic constitutive modelling. These parameters for brain tissue were determined by Shuck and Advani (1972), and have been used in subsequent

**Table 4**  
Material properties for brain tissue.

Gray and white matters					
Density (kg/m <sup>3</sup> )	Bulk modulus (GPa)	G <sub>0</sub> (kPa)	G <sub>∞</sub> (kPa)	β (s <sup>-1</sup> )	Reference
1040	2.19	528	168	35	(Tse et al., 2014; Shuck and Advani, 1972; Willinger et al., 1999; Stalnaker, 1969)

FEHMs (Tse et al., 2015; Willinger et al., 1999). The parameters for both bulk and shear brain responses are given in Table 4.

#### 2.1.5. PEEK implant

The stress-strain behaviour of semi-crystalline thermoplastic polymers is dictated by the combination of two mechanisms: an intermolecular resistance and a network resistance acting in parallel (Boyce et al., 2000; Haward and Thackray, 1968). The material behaviour of PEEK depends on many mechanical variables such as strain rate, temperature and stress state (Rae et al., 2007). This complex behaviour has been studied by many authors and many constitutive models have been proposed (Chen et al., 2016; El-Qoubaa and Othman, 2016; Garcia-Gonzalez et al., 2015a, 2015b; Garcia-Gonzalez et al., 2017). In this work, the mechanical behaviour of PEEK is defined using the hyperelastic-thermoviscoplastic constitutive model previously developed by Garcia-Gonzalez et al. (2017). This model accounts for pressure dependency, and strain rate and temperature sensitivities within a thermodynamically consistent framework. This model has been calibrated and validated for PEEK for a wide range of loading conditions including impact.

The kinematics basis of the model relies on a multiplicative decomposition of the deformation gradient tensor into thermal ( $\mathbf{F}^0$ ) and mechanical ( $\mathbf{F}^M$ ) parts:  $\mathbf{F} = \mathbf{F}^M \mathbf{F}^0$ . While the mechanical contribution of the network resistance is assumed to behave as purely elastic, the mechanical contribution of the intermolecular resistance is assumed to behave elastoplastically. The network resistance contribution to the stress is defined through a hyperelastic spring following the modified eight-chain model proposed by Anand (1996), whereas the one of the intermolecular resistance is defined by a Neo-Hookean spring in series with a viscoplastic dashpot activated when a yield function based on the Raghava equivalent stress is satisfied.

The details of this constitutive model and its material parameters for PEEK can be found in the work of Garcia-Gonzalez et al. (2017).

#### 2.1.6. Macroporous HA implant

The mechanical properties of macroporous HA vary considerably with the porosity of the material, the size and the distribution of the pores (Hing et al., 1999). The lack of knowledge and literature about the mechanical properties of the exact macroporous HA material employed in cranial implants made it necessary to conduct characterisation tests on specimens manufactured from a real prosthesis.

**2.1.6.1. Mechanical characterization of macroporous HA.** Specimens were manufactured from a cranial implant (Custombone, Finceramica, Italy). As these implants are curved, regions of low curvature were first selected in order to produce specimens. Square sections were cut from these regions, which were then ground into cylinders of 10 mm diameter and 6 mm height; exact heights varied but were measured for each specimen prior to testing. These specimens were then tested in compression. Preliminary experiments were performed using a commercial screw-driven testing machine (Instron 5982). In view of the small strains-to-failure, displacements were measured using a contacting extensometer attached to the loading platens close to the specimen, and then confirmed using image correlation software (DaVis version 8, LA Vision) to track the deformation of the specimen from a series of photographs taken during the loading. The results for three tests are shown in Fig. 1. They exhibit a high repeatability with the

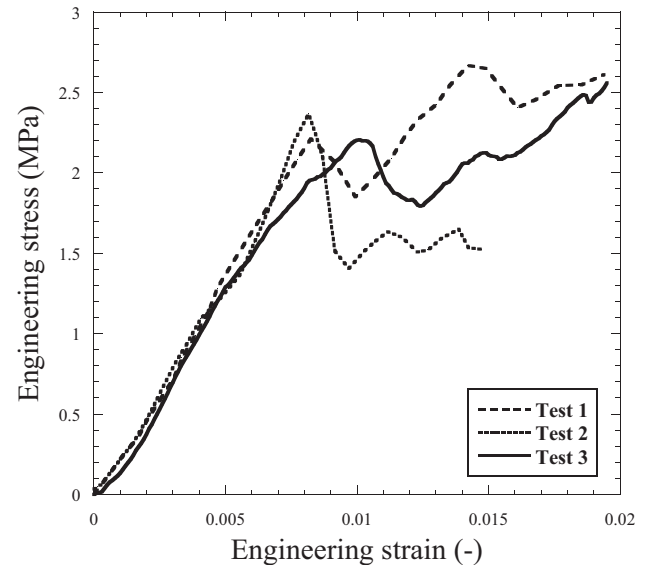


**Fig. 1.** Engineering stress-engineering strain experimental results of the compression tests carried out on macroporous HA specimens.

onset of failure at about 2.2 MPa and an apparent Young's modulus of approximately 0.265 GPa. In order to provide further data for the constitutive model, the material was compressed *in situ* in an X-ray tomography system (Zeiss 510 Versa), using a 5 kN compressive stage (Deben). 360° full scanning with 1601 projections and 85/319 mm of source/detector distances were performed applying  $\times 0.4$  magnification, 14.26  $\mu\text{m}$  pixel size, a source operated at 140 kV and 71  $\mu\text{A}$  and 2 s exposure time. The reconstructed geometries provided the porosity of the specimen, 30%, that, in combination with the measurement of the apparent density of the specimens,  $1,700 \pm 110 \text{ kg m}^{-3}$ , allowed us to determine the density of HA,  $2,500 \text{ kg m}^{-3}$ . In addition, the reconstructed geometries were then used in finite element (FE) simulations described in the next section.

**2.1.6.2. Constitutive modelling of macroporous HA cranial implant.** In order to assess the relevant mechanical properties of the implant, its homogenised behaviour after bone growth needs to be considered. In the first stage, the non-porous HA properties were obtained by reproducing numerically the experimental tests carried out on the specimens manufactured from a real cranial implant. The tomography images taken from a specific specimen allow for the generation of a FE model accounting for a realistic pore distribution, see Fig. 2(a) and (b). The boundary conditions for this model are defined accordingly to the experimental conditions. Under the assumption of linear elastic mechanical response until fracture, the numerical model provides force-displacement curves in a good agreement with the experimental data, see Fig. 2(c). The calibrated values for the Young's modulus and ultimate strength obtained for pure HA are, respectively, 0.75 GPa and 58 MPa.

The experimental results showed a very brittle behaviour of the macroporous HA bioceramic material. This is in agreement with



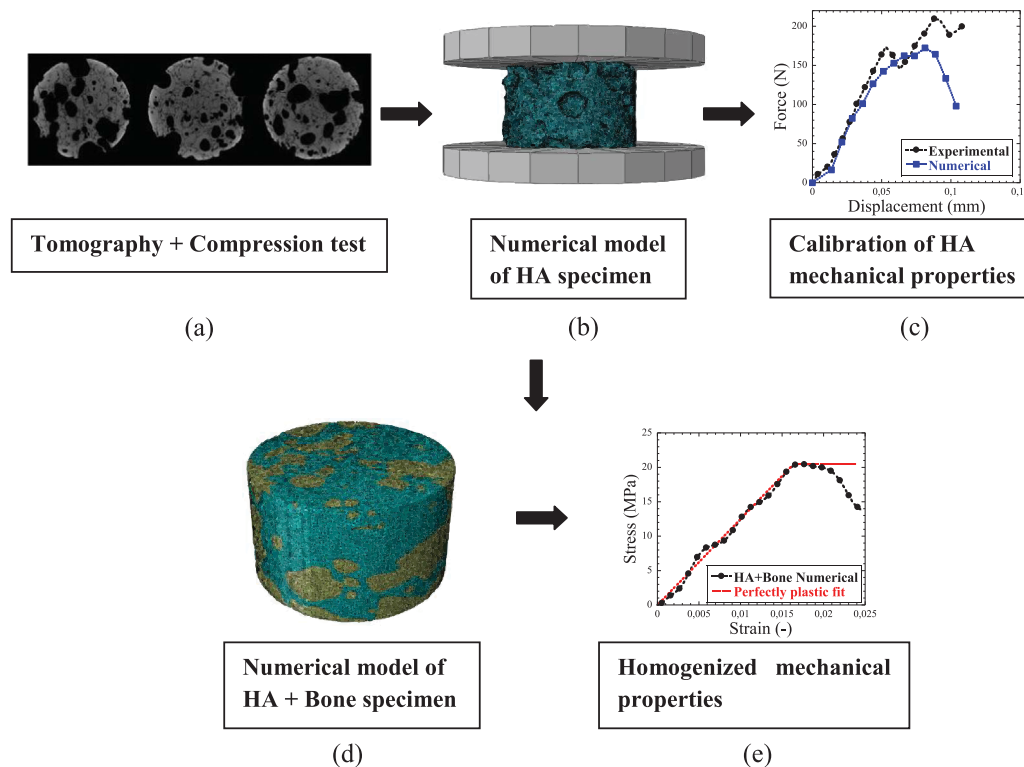


**Fig. 2.** Proposed methodology to obtain the stress-strain behavior of macroporous HA+Bone: a) tomography images of a HA specimen are retrieved; b) from which a numerical model of HA compression test is built; c) and calibrated against experimental force-displacement curves; d) a numerical model of HA+Bone specimen is then created by filling the pores with bones; e) the resulting numerical model predictions are used to calibrate the proposed homogenised model for HA+Bone mechanical behaviour.

previous studies on ceramic materials (Hing et al., 1999). However, it has been observed that when reinforcement is added into a ceramic matrix, not only is the fracture toughness significantly increased but also the propensity for catastrophic failure is reduced (Deng et al., 2016). In this regard, the composite HA+Bone can be considered as a particulate reinforced material composite where HA acts as the matrix and bone as the reinforcement. In such materials, a common assumption is to consider that the composite yielding or breaking starts when, in any material point inside the matrix phase, the yield stress or ultimate strength are reached (Zahr Viñuela and Pérez-Castellanos, 2015). In this work, the ultimate strength of the homogenised HA+Bone was obtained following this assumption since it is the most conservative one.

Under the assumption that the macroporous HA material filled with bone is going to fail through the matrix, a numerical model of the HA+Bone specimen was developed by substituting the pores of the previous HA model for bone, see Fig. 2(d). The boundary conditions applied were the same used as in the model without bone. The properties of cancellous bone were used for bone tissue grown inside the HA pores: a density of  $\rho=1,500 \text{ kg m}^{-3}$ , a Young's modulus of  $E=4.6 \text{ GPa}$  and a Poisson's ratio of  $\nu=0.05$  (Sahoo et al., 2014). This numerical model was finally used for the evaluation of the macroscopic mechanical properties of the HA+Bone specimen as a whole, see Fig. 2(e). The homogenised density, Young's modulus and ultimate strength were found to be  $2,224.65 \text{ kg m}^{-3}$ ,  $1.25 \text{ GPa}$  and  $20.50 \text{ MPa}$ , respectively. A summary of the constitutive assumptions used in this work is presented in Appendix A.

## 2.2. Finite element human head

### 2.2.1. Geometry and mesh generation from MRI

In this work, a detailed finite element model of a human head has been developed in order to study the suitability of two different cranial implants subjected to impact loads. The head model comprises the

scalp, the skull, the cerebral falx, the CSF, the ventricles, the brain and a cranial implant replacing part of the skull, see Fig. 3(a). The geometrical information was obtained from full-head, high resolution anatomical T1 and T2-weighted MRI images of a subject available from the Human Connectome Project (HCP Subject ID: 100307) (Van Essen et al., 2013). The anatomical images were used as input to “BET2” (Smith, 2002; Jenkinson et al., 2005) in the FSL software library (Smith et al., 2002), to extract inner skull, outer skull and outer scalp surfaces. The skull-stripped brain was further segmented into white matter, gray matter and ventricles using the Amira software (FEI Amira 6.0.1, 2015). In order to guarantee the anonymity of the patient from which the images were obtained, the MRI images are released “de-faced” by the HCP (Milchenko and Marcus, 2013), i.e. blurred at the eyes, nose and ears. These parts in the scalp and skull components were manually reconstructed in our model without affecting the brain. The implant geometry was designed in accordance with the average dimensions used when dealing with unilateral decompressive craniectomy.

The resulting multi-component (see Fig. 3) optimised FE model weighs  $3.91 \text{ kg}$  and is composed of  $792,773$  tetrahedral elements, for which spatial convergence was verified.

### 2.2.2. Loading conditions

In order to study the load-bearing capacity of the structural prostheses and their effectiveness in protecting brain tissues, simulations have been conducted for impact conditions representative of falls. Many scenarios involving the fall of a person result in serious head injuries. A common scenario is the fall from bed, where the head is usually the most frequent body part injured (Sadigh et al., 2004). Schulz et al. (2008) reproduced falls from a bed and obtained, for an impact of  $4.2 \text{ m s}^{-1}$ , a resultant head velocity normal component to ground between  $3.44 \text{ m s}^{-1}$  and  $3.86 \text{ m s}^{-1}$ . Another example of fall which involves serious head injuries is observable in bicycle accidents. A fall from a bike can occur in many different ways and the variation of

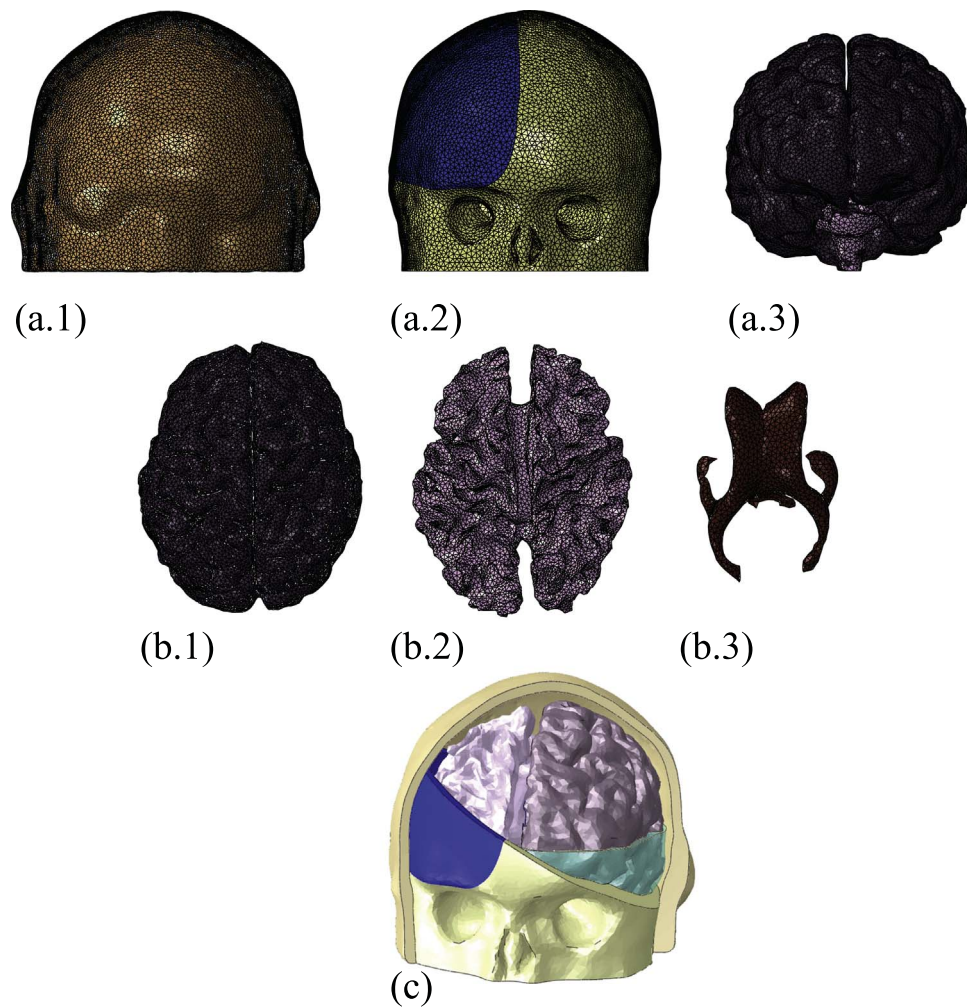


**Fig. 3.** Full head finite element model showing various components: (a.1) scalp; (a.2) skull+implant; (a.3) brain tissues; (b.1) gray matter; (b.2) white matter; (b.3) ventricles; (c) whole head model.

kinematics, head orientation and velocity can be large (Fahlstedt et al., 2012). Fahlstedt et al. (2012) simulated a real bike accident and obtained a resultant linear velocity of the head just before impact of  $5.3 \text{ m s}^{-1}$  with a normal component to ground of  $4 \text{ m s}^{-1}$ . The FEHM presented here was validated in terms of kinematics against three scenarios and the impact velocity range was thus defined from  $1 \text{ m s}^{-1}$  to  $7 \text{ m s}^{-1}$  covering the range observed in these different falls. The simulations herein were carried out by using the FE solver Abaqus (2012).

The mechanical response of the head was observed to vary depending on the impact location. This fact is basically due to the non uniformity of the skull thickness and the structural influence of its shape. In addition, in the peripheral zone of the implant, where some screws are located to fix it to the bone, the stresses around the screws can localise with higher values, thus leading to lower impact velocities at which implant fails. Therefore, the head orientation was varied in the simulations with the aim of studying the critical impact velocity which results in implant or skull failure depending on the impact location. As a consequence, the impact locations were chosen along three skull paths: from parietal bone to vertex; from parietal bone to occipital bone; and from parietal bone to frontal bone. The assumption in all simulations is that the body impacts before the head does using the neck as a pivot, thus reducing the inertial effects to the weight of the head.

For the analysis of the implant effectiveness in protecting brain tissue, a specific impact scenario was selected as worst-case reference

for comparison. For this purpose, an orientation angle of  $30^\circ$  between head and ground was selected because a) it was found to be the critical value which introduces a perpendicular impact directly on the implant and, b), it is in the parietal zone where the skull thickness is thinner, see Fig. 4.

The ground was defined as a rigid body since it is much stiffer than the head tissues. Following Fahlstedt et al. (2012), this contact was modelled with a penalty contact algorithm with a constant friction coefficient value set to 0.4.

### 2.2.3. Injury criteria and evaluation procedure

In this work, the effectiveness of each implant is determined following two methodologies: the structural integrity of the implant and the potential TBI.

Material fracture and plastic deformation have been established as reliable indicators of structural integrity (Goh and Lee, 2002). When dealing with a general case where the influence of screws in the stress distribution along the implant is neglected, fracture and plastic deformation are estimated at the macroscale by the ultimate strength and yield stress of the material used. The ultimate strength for bone has been estimated to be  $92.72 \text{ MPa}$  (Wood, 1971; Zhou et al., 2016). For HA+Bone this value is evaluated to be  $20.50 \text{ MPa}$  from the analysis carried out earlier. In PEEK, the deformation experienced along the impact process is more localised than in the case of HA or bone because its ductile behaviour. It results in different strain rates along the PEEK

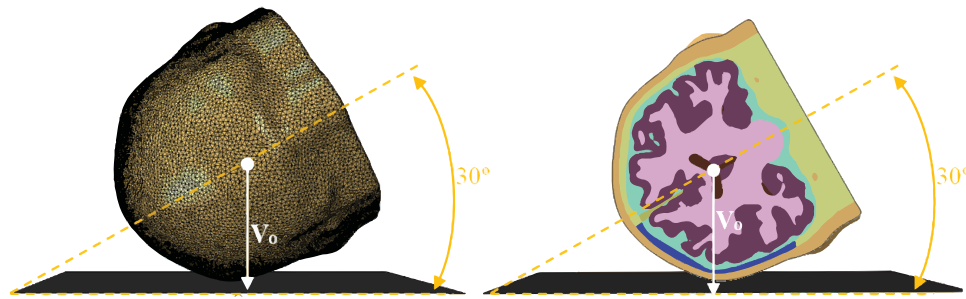


**Fig. 4.** Boundary and initial conditions for the critical impact study on the parietal zone (orientation angle of 30° between head and ground).

implant structure and, consequently, different stress thresholds to reach yielding because of its rate-dependent properties. Since a constitutive model has been defined taking into account rate dependencies, it can be determined when the PEEK implant reaches yielding depending on the strain rate in each zone. Moreover, when the impact takes place close to the peripheral zone of the implant, the effect introduced by the screws in concentrating the stress must be considered. As the FEHM does not include the screws, a complementary analysis is done in order to capture the stress concentration effect which should be applied to the surroundings of the screws location.

To this end, a numerical model of a representative volume of the bone-implant interface has been developed and the stress distribution was analysed when screws are considered and when they are not. Different stress states were applied to a 120×60×6 mm<sup>3</sup> plate. The thickness of the plate was selected to be representative of the skull and the other two dimensions were optimised to avoid introducing a geometrical influence on the stress distribution. These results were compared with simulations under the same conditions but including two screws of 1.5 mm rigidly attached together with a distance of 12 mm between them. Thus, the concentration ratio to be applied in the peripheral zone of the implant was selected as the maximum one found from uniaxial compression; uniaxial tension; shearing; and out-of-plane stress states. The concentration ratio for the bone zone affected by the screws was found equal to 1.29; the average one for the PEEK zone affected by the screws was found equal to 1.28; and the one for the HA zone affected by the screws was found equal to 1.32.

In order to define a common framework to analyse the efficiency of both implants in protecting the brain against impact loads, some indicators have been used for TBI assessment in terms of mechanical variables such as pressure, shear stress, von Mises stress and strain. These post-traumatic biomechanical parameters are compared with brain tissue tolerance thresholds in the literature as collected by Tse et al. (2014), see Table 5. Following the methodology presented by these authors, the critical anatomical locations are reported and a dimensionless parameter is used as a mechanical equivalent of brain injuries. This dimensionless parameter is defined in a similar way as the cumulative strain damage measure proposed by Takhounts and Eppinger (2003). It is thus chosen as the ratio between the number of elements reaching the critical value associated to damage and the total number of elements which compose the brain tissue.

### 3. Results and discussion

Numerical simulations of impacts on the FEHM were conducted for an impact velocity range of 1 m s<sup>-1</sup> to 7 m s<sup>-1</sup> for three possible scenarios: when the subject has a PEEK implant; when the subject has a HA implant; and when the subject's skull presents no previous damage. The results and discussion of these simulations are introduced in three sections: acceleration-time predictions, critical impact velocity predictions, and TBI predictions.

**Table 5**

Thresholds of brain injury criteria (Tse et al., 2014).

Parameter	Thresholds	Reference
Pressure	<b>Criterion 1</b> > 235 kPa→injury < 173 kPa→minor or no injury	(Ward et al., 1980)
Shear stress	<b>Criterion 2</b> 11–16.5 kPa→severe injury	(Kang et al., 1997)
Von Mises stress	<b>Criterion 3</b> > 18 kPa→50% probability of moderate neurological lesions > 38 kPa→50% probability of severe neurological lesions <b>Criterion 4</b> ≥26 kPa→axonal damage	(Baumgartner and Willinger, 1997) (Deck and Willinger, 2008)
Strain	<b>Criterion 5</b> > 0.25→structural damage > 0.20→functional damage > 0.10→reversible damage	(Galbraith et al., 1993)

#### 3.1. Acceleration-time validation

In this section, the model predictions for acceleration-time curves are compared with available data from the literature in order to ensure that the impact conditions imposed are representative of real accidents and falls. In addition, a comparison between the mechanical response of the head when PEEK implant, HA implant and no implant are incorporated, is done in terms of acceleration-time curves. Three cases are considered here for comparison. Schulz et al. (2008) reported experimental data of the fall of a person from a bed and Fahlstedt et al. (2012) reported numerical data of a bike accident reconstruction. The resultant velocity component in the perpendicular direction to the ground was estimated between 3.44 m s<sup>-1</sup> and 3.86 m s<sup>-1</sup> for the fall from the bed and 4 m s<sup>-1</sup> for the bike accident. The third set of data corresponds to measurements performed during experiments in which human heads cut from cadavers were impacted against a rigid plate (Loyd et al., 2014).

In Fig. 5(a), the model predictions for the acceleration-time curves of the perpendicular head drops when no implant is included in the FEHM are compared with literature data. The numerical acceleration-time data presented herein were obtained from the force-time curves by dividing the force values by the mass of the whole head. It can be observed that both fall from the bed and bike accident cases are within the impact velocity and acceleration ranges simulated. The effective impact velocity estimated by Loyd et al. (2014) was 2.42 m s<sup>-1</sup> and the head drop was conducted on the vertex location. The model prediction shows a slightly overestimation of the maximum acceleration reached compared with the experiment. This can be explained by the lower mass of the head tested post-mortem (≈3.2 kg) thus implying a lower inertial contribution to the impact process. From the results shown in Fig. 5(a), it can be concluded that the model predictions conducted

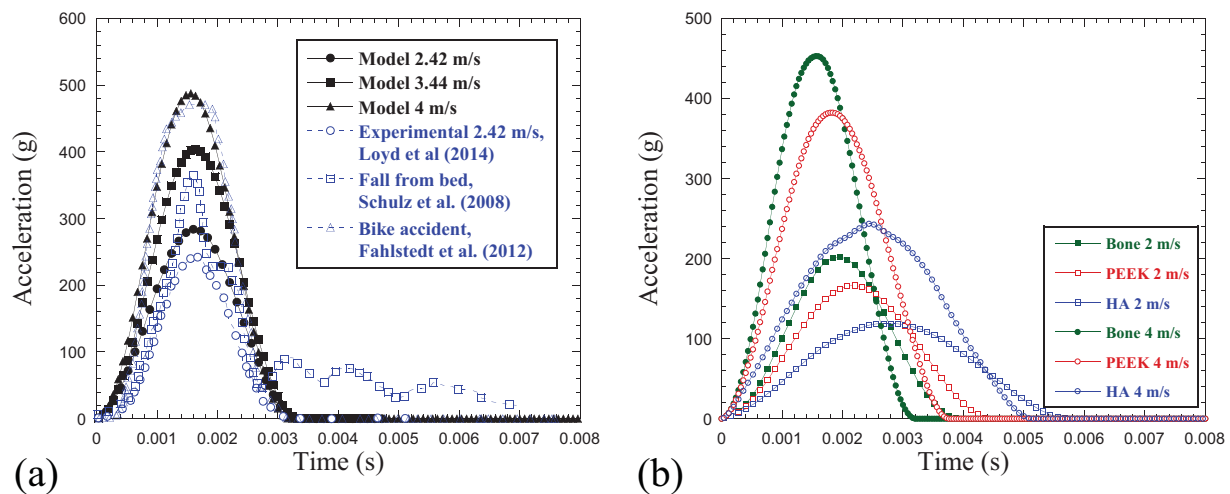


Fig. 5. Acceleration-time numerical predictions of the model: (a) comparison with published data; and (b) comparison between PEEK implant, HA implant and no implant predictions.

cover the impact velocity and acceleration ranges found in common accidents which involve head impacts.

Moreover, the acceleration-time response of the human head during impact was analysed for both PEEK and HA. The results, presented in Fig. 5(b), show the higher peaks of acceleration for PEEK at  $2 \text{ m s}^{-1}$  and  $4 \text{ m s}^{-1}$  impact velocities. In contrast, the deformation experienced by the implant is more significant for HA. This is consistent with the lower HA Young's modulus, which also results in a prolongation of the contact duration. While the use of a softer material for the implant results in a major deformation and thus trauma, it also implies a higher damping effect in reducing brain motion.

### 3.2. Critical impact velocity predictions inducing implant failure

When considering the conditions for implant failure during impacts, two factors have to be taken into account: the impact velocity and the impact location. An increase in the impact velocity implies a higher impact energy leading to higher stresses in the implant. This results in a higher risk of implant failure as the impact velocity increases. The impact location plays an important role not only because of the variation of thickness and the variation of structural stiffness along the skull, but also because of the presence of screws and their role in concentrating the stress. As a consequence, a parametric study varying both impact velocity and impact location was carried out along three different paths covering the most common impact scenarios in fall accidents. This study allows us to estimate the impact velocity which is expected to result in implant failure for all the scenarios considered.

The three skull paths are: from parietal bone to vertex (Fig. 6(a.1)); from parietal bone to occipital bone (Fig. 6(a.2)); and from parietal bone to frontal bone (Fig. 6(a.3)). The critical impact velocity resulting in implant failure for each point is presented in Fig. 6(b) for PEEK implant and in Fig. 6(c) for HA+Bone implant. In both cases the parietal-vertex path is the weakest. In addition, there is a direct relationship between critical impact velocity and distance to implant interface, where the implant-bone interface where the screws are located is the weakest and most critical zone. For the parietal-vertex and parietal-occipital paths, the critical impact velocity presents a minimum at the implant-bone interface (0 mm) due to the presence of the screws. As the distance between impact location and the implant-bone interface increases, the critical impact velocity continuously increases until reaching the critical impact velocity of the impacted material. However, while the parietal-frontal path also shows a minimum in the implant-bone interface, the impact velocity does not present a continuous increase by augmenting the distance to the main

interface (0 mm). This is due to the closeness of the lower interface of the implant, which is also affected by the possible presence of screws. Accordingly, it can be established that lower velocities can result in implant failure if the impact takes place closer to the peripheral zone of the implant where the fixation system to bone is located. Note that the proposed approach does consider a continuous distribution of screws along the interface instead of just a few. This implies that the results presented here are “worst-case scenarios”.

The mechanical properties of the material used in the implant are found to play the predominant role in avoiding implant failure. For all the scenarios tested, the PEEK implant exhibits a better mechanical response against impact loading than the HA+Bone implant. A good indicator of the load bearing capacity of these materials is the critical impact velocity resulting in implant failure when the impact takes place far enough from the peripheral zone of the implant where the effect of the screws can be neglected. In this regard, this velocity was determined from impact simulations with an orientation angle of  $30^\circ$  between the head and ground where the PEEK implant, the HA+Bone implant and no implant were considered (see Fig. 4). The critical impact velocity for PEEK was found to be  $6.5 \text{ m s}^{-1}$  and, in the case of bone and HA+Bone it was found to be 54% and 80% lower, respectively. The difference between PEEK and HA+Bone in terms of energy absorption capability results in different implant failure patterns. When a PEEK implant is employed and subjected to an impact, the implant failure occurs predominantly in the onlay-structure (the closest zone of the bone to the implant interface) where the bone part is fixed by the screws, and even in some situations in which the impact takes place in the implant zone. However, when a HA+Bone implant is employed, the implant failure occurs predominantly in the inlay-structure of the implant zone instead of the bone. It must be noticed that the critical impact velocities resulting in implant failure have been obtained for a case where the ground is considered rigid. This assumption corresponds to the most critical situation.

Overall, these results suggest that the biomaterial to be used for the cranial implant should be selected depending on the specific patient and his exposure to impact loadings. In this regard, the macroporous HA+Bone implant is observed to behave in a very brittle way when it is subjected to impacts of different natures. This brittle behaviour and associated catastrophic failure of the HA implant has already been reported by Adetchessi et al. (2012), who presented a clinical case of a 25-year-old man. After a cranioplasty using macroporous HA prosthesis, the patient had to undergo a second surgery following an implant failure due to an impact during a generalised seizure. In the second intervention a PEEK solution was finally used.



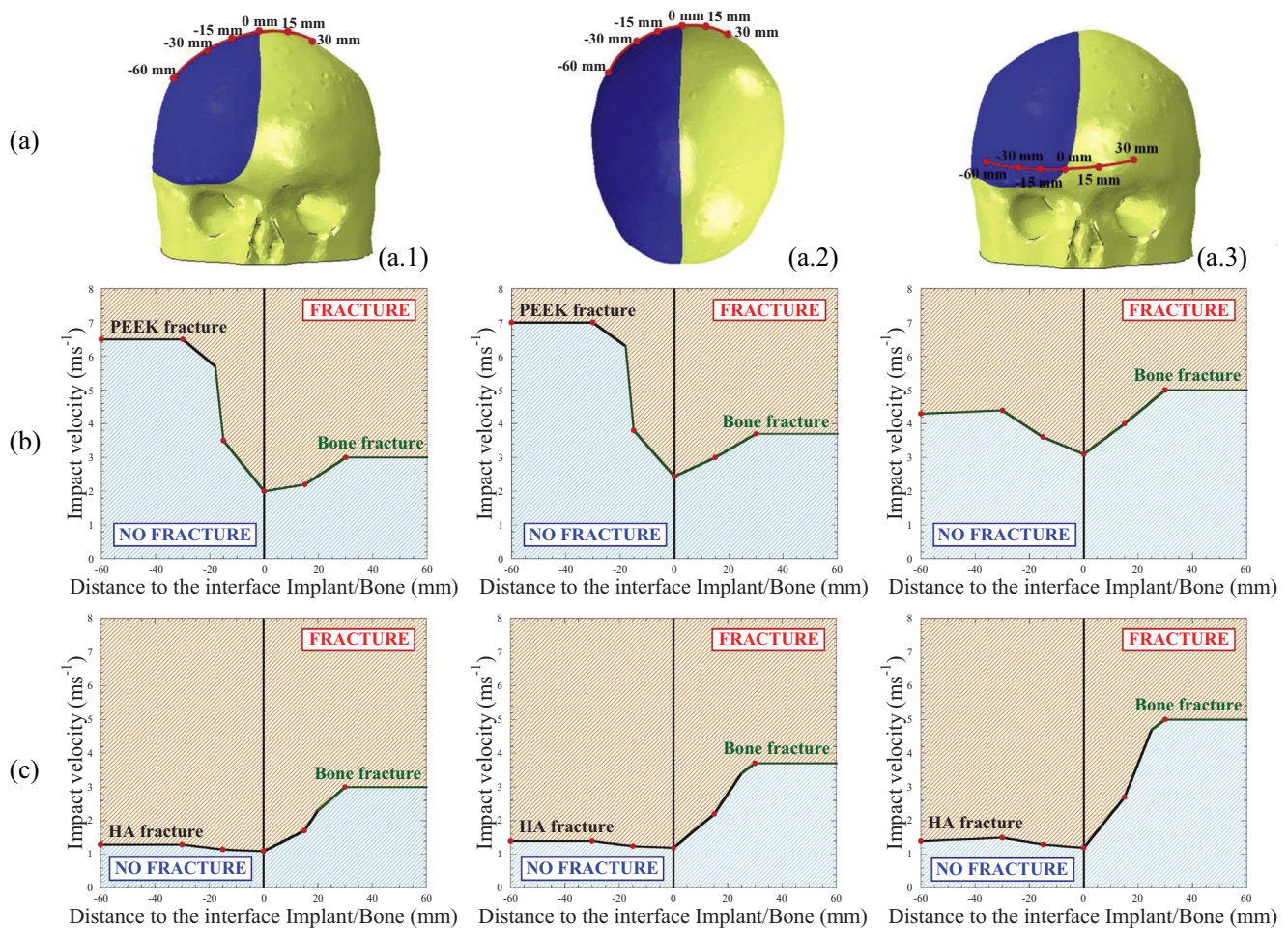


**Fig. 6.** (a) Impact localisation points defined along the three skull paths studied: (a.1) parietal-vertex; (a.2) parietal-occipital; and (a.3) parietal-frontal. Risk of fracture as a function of impact velocity and distance to the implant interface along different paths for: (b) PEEK implant; and (c) HA implant. (Only the skull and implant are shown.)

### 3.3. TBI predictions

Since the main function of the implant is to protect the brain against external loads, the effectiveness of both implants in avoiding TBI is compared here. In the biomechanics community, the risk of TBI has been determined based on intracranial biomechanical parameters. The aim of this paper is not to determine the most suitable criterion for evaluating TBI. Instead, this section focusses on comparing the effectiveness of both cranial implants by applying different criteria proposed in previous studies, see Table 5. Therefore, as mentioned previously, a dimensionless parameter providing the percentage of brain tissue with probability of damage is determined for each biomechanical parameter depending on the impact velocity. For this study, an orientation angle between the head and ground of  $30^\circ$  leading to a perpendicular impact on the implant has been adopted as a common impact scenario for comparison, see Fig. 4. More details on the predictive variables, thresholds and boundary conditions used in these numerical simulations are provided in Appendix B.

The results are provided in Fig. 7. The intracranial pressure based criterion (Criterion 1) was found not to vary significantly between the two implants studied because the threshold values are reached in almost the whole brain at relatively low impact velocities (lower than  $3 \text{ m s}^{-1}$ ), and is not studied further here. For the remaining criteria, a higher TBI level for macroporous HA+Bone implant than for PEEK

implant is observed. In Fig. 7, the percentages of damaged tissue as a function of impact velocity are presented for the remaining criteria.

TBI can be understood as a combination of the deformation processes due to brain motion and indentation process on the skull. In this regard, the stiffness of the material used in the implant, defined by its Young's modulus, plays a predominant role in the brain deformation. On the one hand, a lower stiffness has a beneficial effect due to its higher damping effect of the implant which results in a reduction of the brain motion. This damping effect is easily observed in the results shown in Fig. 5(b), where a lower material stiffness results in lower acceleration values and in a prolongation of the contact duration. On the other hand, a lower stiffness leads to a larger trauma by a more important deflection of the implant directly affecting the brain tissue. Fig. 8 shows the anatomical location and extension of severe brain damage in dark colours and moderate brain damage in light colours according to Criterion 3, see Table 5. It can be observed that the predominant deformation is produced by the implant bending and is localised at the contact zone where the impact takes place. A direct relationship is here established between the Young's modulus of the material used for the implant and the effectiveness of the prosthesis in avoiding TBI under the specified loading conditions. In this case, bone is the best TBI protective material, followed by PEEK, and eventually the HA + Bone implant.

Finally, it is worth noting that since PEEK shows a much better behaviour in terms of energy absorption capability with respect to bone

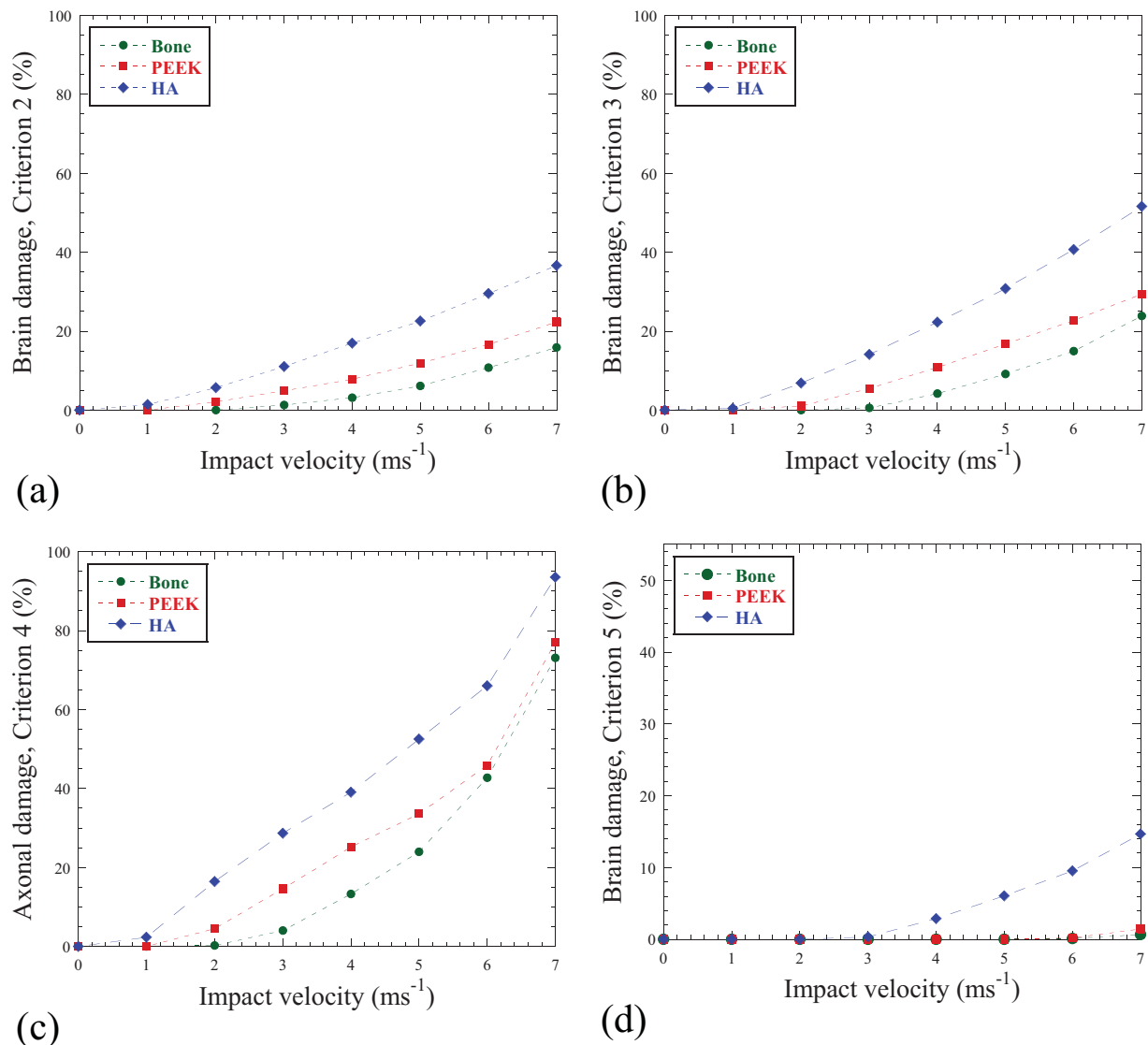


**Fig. 7.** Percentage of damaged elements in brain tissue vs. impact velocity based on: (a) Criterion 2; (b) Criterion 3; (c) Criterion 4; and (d) Criterion 5. Predictions conducted for critical impact conditions shown in Fig. 4.

but as its lower stiffness results in a worse protection against TBI, a good alternative can be the reinforcement of PEEK matrix with short fibres (Garcia-Gonzalez et al., 2015a, 2015b). Such approach balances the excess of energy absorption capacity and the lack of stiffness in comparison with bone. Furthermore, it can be manufactured by injection moulding allowing for the customisation of implant designs, and its biocompatibility and suitability for cranioplasty have been demonstrated (Piitulainen et al., 2015; Posti et al., 2016).

#### 4. Conclusions

A numerical head model from anonymous MRI has been developed and used to compare the mechanical behaviour under impact loading of two cranial implants: PEEK and macroporous HA+Bone. The model was validated in terms of the kinematics of head under impact conditions and used to:

- (i) Compare the mechanical response of the two cranial implants under a wide range of impact conditions. In terms of implant failure and TBI, the numerical results showed a better mechanical behaviour of PEEK implant under the loading conditions tested.

Additionally, a high risk of fracture was found when a HA implant is subjected to impact loading.

- (ii) Provide a roadmap for the determination of the risk of implant failure when the subject has been exposed to any accident involving impact loading.

There are of course many clinical considerations when choosing a cranial implant. These include cost, availability and timescales, among others. Manufacturers of such implants are frequently found to claim greater biointegration, lower infection rates, easier implant techniques and other rather hard-to-demonstrate benefits. Eventually, an implant is required to provide: a) protection with b) an acceptable cosmetic result. Both HA and PEEK (among others) provide these. However, patients receiving implants are more likely to suffer from neurological deficits and epilepsy than the general population, and these both increase the risks of falls, and injury to the implant and underlying brain. Additionally, the patients that have made a good enough recovery may well wish to go back to sports and exercise, which may well increase these risks further. As a conclusion, a patient specific assessment of what the implant will need to withstand in the future is recommended to tailor the choice of implant accordingly.

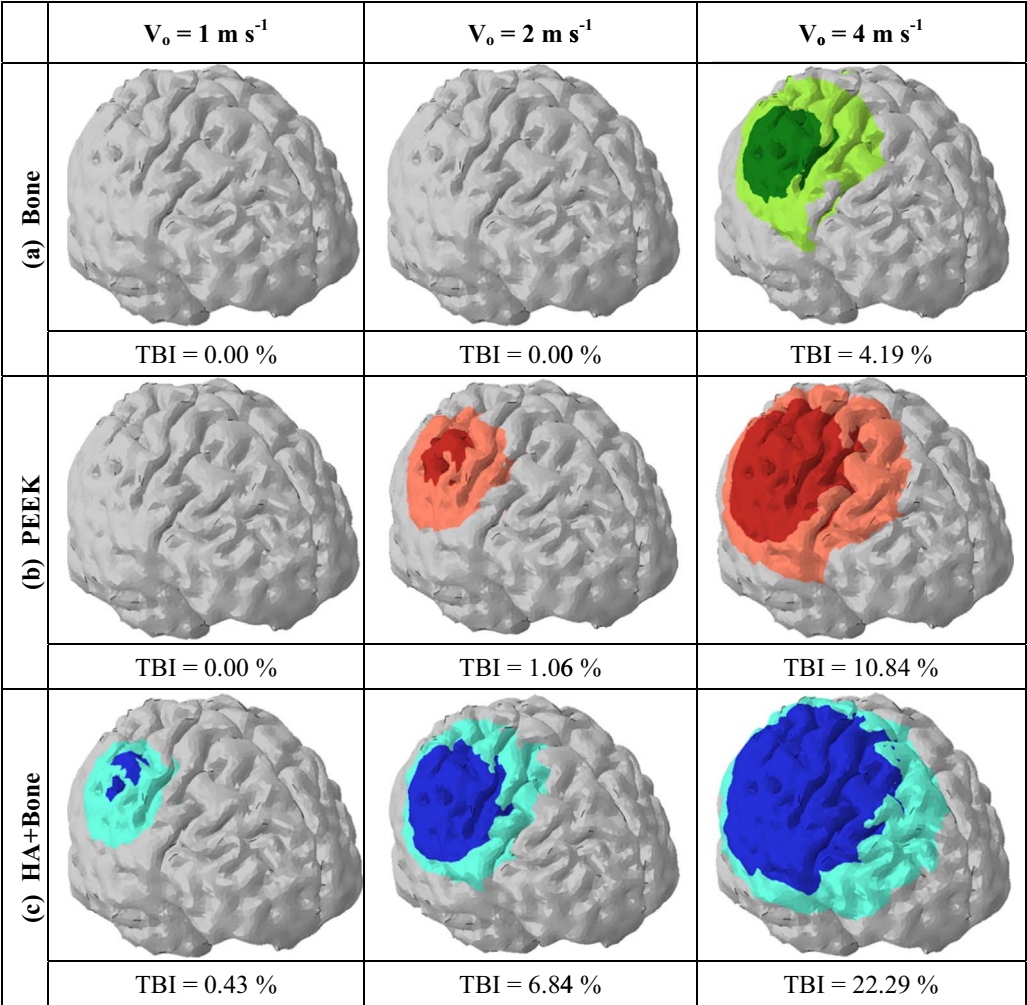


**Fig. 8.** Severe brain damage (dark colours and TBI percentages) and moderate damage (light colours) according to Criterion 3 at impact velocities of 1 m/s, 2 m/s and 4 m/s: (a) no implant; (b) PEEK implant; and (c) HA implant. Predictions conducted for critical impact conditions shown in Fig. 4. (For interpretation of the references to color in this figure legend, the reader is referred to the web version of this article.)

**Conflict of interest**

The authors confirm that there are no known conflicts of interest associated with this publication and there has been no significant financial support for this work that could have influenced its outcome.

**Acknowledgements**

The researchers of the University Carlos III are indebted to the Ministerio de Economía y Competitividad de España (Project DPI2014-57989-P) and Vicerrectorado de Política Científica UC3M (Project 2013-00219-002) for the financial support.  
A.J. acknowledges funding from the European Union's Seventh

Framework Programme (FP7 2007–2013) ERC Grant Agreement No. 306587.  
MRI data were provided by the Human Connectome Project, WU-Minn Consortium (Principal Investigators: David Van Essen and Kamil Ugurbil; 1U54MH091657) funded by the 16 NIH Institutes and Centers that support the NIH Blueprint for Neuroscience Research; and by the McDonnell Center for Systems Neuroscience at Washington University. Finally, we would like to thank Dr. S Barhli and Prof. J Marrow for valuable assistance with the X-ray tomography; the machine used was bought from EPSRC Grant EP/M02833X/1 “University of Oxford: experimental equipment upgrade”.

**Appendix A. Constitutive assumptions**

The constitutive assumptions for each head tissue and biomaterial are provided in Table A.1.



**Table A.1**  
Constitutive assumptions of the FEHM.

Tissue/biomaterial	Constitutive law	Reference
Scalp	Linear elastic	(Horgan and Gilchrist, 2003; Liu et al., 2007; Sahoo et al., 2014 Zhang et al., 2001)
Skull	Linear elastic	(Wood, 1971)
Falx	Linear elastic	(Chafi et al., 2010; Takhounts et al., 2008)
CSF	Equation of state+Newtonian viscosity	Water (e.g., Jérusalem and Dao, 2012)
Ventricles	Equation of state+Newtonian viscosity	Water (e.g., Jérusalem and Dao, 2012)
Gray and white matters	Viscoelastic	(Tse et al., 2014; Shuck and Advani, 1972; Willinger et al., 1999; Stalnaker, 1969)
PEEK	Hyperelastic-Thermoviscoplastic	(Garcia-Gonzalez et al., 2017)
HA+Bone	Linear elastic until fracture	This work

**Appendix B. Details of predicted variables, thresholds and boundary conditions used in the numerical simulations conducted for evaluating TBI**

The predicted variables, thresholds and boundary conditions used in the numerical simulations conducted in the evaluation of TBI are schematically provided in Table B.1.

**Table B.1**  
Predicted variables, thresholds and boundary conditions used in the numerical simulations conducted for TBI evaluation.

Predicted variables		Thresholds	Boundary conditions
Criterion 1	Pressure	235 kPa	Impact velocity from 0 m/s to 7 m/s Orientation angle of 30° between head and ground
Criterion 2	Shear stress	11 kPa	
Criterion 3	Von Mises Stress	38 kPa	
Criterion 4	Von Mises Stress	26 kPa	
Criterion 5	Strain	0.25	

**References**

Adetchessi, A.T., Pech-Gourg, G., Metellus, P., Fuentes, S., 2012. Fracture précoce d'une cranioplastie en céramique macroporeuse d'hydroxyapatite. *Neurochirurgie* 58, 382–385.

Al-Bsharat, A.S., Hardy, W.N., Yang, K.H., Khalil, T.B., Tashman, S., King, A.I., 1999. Brain/skull relative displacement magnitude due to blunt head impact: new experimental data and model. In: *Proceedings of the 1999 43rd Stapp Car Crash Conference*; San Diego, CA, USA P-350, pp. 321–332

Anand, L., 1996. A constitutive model for compressible elastomeric solids. *Comput. Mech.* 18, 339–355.

Annaiidha, A.N., Bruyèred, K., Destradea, M., Gilchrist, M.D., Otténiod, M., 2012. Characterization of the anisotropic mechanical properties of excised human skin. *J. Mech. Behav. Biomed. Mater.* 5, 139–148.

Baumgartner, D., Willinger, R., 2005. Human head tolerance limits to specific injury mechanisms inferred from real world accident numerical reconstruction. *Rev. Eur. Élé.* 14, 421–443.

Boyce, M.S., Socrate, S., Llana, P.G., 2000. Constitutive model for the finite deformation stress–strain behavior of poly(ethylene terephthalate) above the glass transition. *Polymer* 41, 2183–2201.

Boyde, A., Corsi, A., Quarto, R., Cancedda, R., Bianco, P., 1999. Osteoconduction in large macroporous hydroxyapatite ceramic implants: evidence for a complementary integration and disintegration mechanism. *Bone* 24, 579–589.

Budday, S., Nay, R., de Rooij, R., Steinmann, P., Wyrobek, T., Ovaert, T.C., Kuhl, E., 2015. Mechanical properties of gray and white matter brain tissue by indentation. *J. Mech. Behav. Biomed. Mater.* 46, 318–330.

Chafi, M.S., Karami, G., Ziejewski, M., 2010. Biomechanical assessment of brain dynamic responses due to blast pressure waves. *Ann. Biomed. Eng.* 38, 490–504.

Chen, F., Ou, H., Lu, B., Long, H., 2016. A constitutive model of polyether-ether-ketone (PEEK). *J. Mech. Behav. Biomed. Mater.* 53, 427–433.

Chistolini, P., Ruspantini, I., Bianco, P., Corsi, A., Cancedda, R., Quarto, R., 1999. Biomechanical evaluation of cell-loaded and cell-free hydroxyapatite implants for the reconstruction of segmental bone defects. *J. Mater. Sci. Mater. Med.* 10, 739–742.

Dassault Systèmes Abaqus v6.12, 2012. *Documentation-ABAQUS Analysis User's Manual*, Abaqus Inc.

Deck, C., Willinger, R., 2008. Improved head injury criteria based on head FE model. *Int. J. Crashworthiness* 13, 667–678.

Deng, Y., Li, W., Wang, R., Shao, J., Geng, P., Ma, J., 2016. The temperature-dependent fracture models for fiber-reinforced ceramic matrix composites. *Compos. Struct.* 140, 534–539.

Doblaré, M., García, J.M., Gómez, M.J., 2004. Modelling bone tissue fracture and healing: a review. *Eng. Fract. Mech.* 71, 1809–1840.

Dunn, M.G., Silver, F.H., 1983. Viscoelastic behavior of human connective tissues: relative contribution of viscous and elastic components. *Connect. Tissue Res.* 12, 59–70.

El Halabi, F., Rodriguez, J.F., Rebolledo, L., Hurtós, E., Doblaré, M., 2011. Mechanical characterization and numerical simulation of polyether-ther-ketone (PEEK) cranial implants. *J. Mech. Behav. Biomed. Mater.* 4, 1819–1832.

El-Qoubaa, Z., Othman, R., 2016. Strain rate sensitivity of polyetheretherketone's compressive yield stress at low and high temperatures. *Mech. Mater.* 95, 15–27.

Eolchiyan, S.A., 2014. Complex skull defects reconstruction with CAD/CAM titanium and polyetheretherketone (PEEK) implants. *Zhurnal Vopr. Neurokhirurgii Im. N.N. Burdenko* 75, 3–13.

Fahlstedt, M., Baeck, K., Halldin, P., Sloten, J.V., Goffin, J., Depreitere, B., Kleiven, S., 2012. Influence of impact velocity and angle in a detailed reconstruction of a bicycle accident. In: *Proceedings of the ICORBI Conference*, 84, pp. 787–799

FEI Amira 6.0.1, 2015.

Frassanito, P., De Bonis, P., Mattogno, P.P., Mangiola, A., Novello, M., Brinchi, D., Pompucci, A., Anile, C., 2013. The fate of a macroporous hydroxyapatite cranioplasty four years after implantation: macroscopical and microscopical findings in a case of recurrent atypical meningioma. *Clin. Neurol. Neurosurg.* 115, 1496–1498.

Fredriksson, R., Håland, Y., Yang, J., 2001. Evaluation of a new pedestrian head injury protection system with a sensor in the bumper and lifting of the bonnet's rear part. In: *Proceedings of the 17th ESV Conference*, Amsterdam, Netherlands

Galbraith, J.A., Thibault, L.E., Matteson, D.R., 1993. Mechanical and electrical responses of the squid giant axon to simple elongation. *J. Biomech. Eng.* 115, 13–22.

Gambardotta, L., Massabo, R., Morbiducci, R., Raposio, E., Santi, P., 2005. In vivo experimental testing and model identification of human scalp skin. *J. Biomech.* 38, 2237–2247.

Gao, C., 2007. *Finite Element Modelling of the Human Brain and Application in Neurosurgical* (Ph.D. dissertation), Singapore

Garcia-Gonzalez, D., Zaera, R., Arias, A., 2017. A hyperelastic-thermoviscoplastic constitutive model for semi-crystalline polymers: application to PEEK under dynamic loading conditions. *Int. J. Plast.* 88, 27–52.

Garcia-Gonzalez, D., Rusinek, A., Jankowiak, T., Arias, A., 2015a. Mechanical impact behavior of polyether–ether–ketone (PEEK). *Compos. Struct.* 124, 88–99.

Garcia-Gonzalez, D., Rodriguez-Millan, M., Rusinek, A., Arias, A., 2015b. Investigation of mechanical impact behavior of short carbon-fiber-reinforced PEEK composites. *Compos. Struct.* 133, 1116–1126.

Giovanni, B., Chiandussi, G., Gaviglio, I., 2005. Development and validation of a new finite element model of human head. In: *Proceedings of the 19th International Technical Conference on the Enhanced Safety of Vehicles (ESV)*, Washington, D.C., Paper No. 05-0441

Goh, J.C.H., Lee, P.V.S., Ng, P., 2002. Structural integrity of polypropylene prosthetic sockets manufactured using the polymer deposition technique. *Proc. Inst. Mech. Eng. H* 216, 359–368.

Goriely, A., Geers, M.G.D., Holzapfel, G.A., Jayamohan, J., Jérusalem, A., Sivaloganathan, S., Squier, W., van Dommelen, J.A.W., Waters, S., Kuhl, E., 2015.



- Mechanics of the brain: perspectives, challenges, and opportunities. *Biomech. Model. Mechanobiol.* 14, 931–965.
- Haward, R.N., Thackray, G., 1968. The use of a mathematical model to describe isothermal stress-strain curves in glassy thermoplastics. *Proc. R. Soc. Lond. Ser. A Math. Phys. Sci.* 302, 453–472.
- Hing, K.A., Best, S.M., Bonfield, W., 1999. Characterization of porous hydroxyapatite. *J. Mater. Sci. Mater. Med.* 10, 135–145.
- Honeybul, S., Ho, K.M., 2016. Predicting long-term neurological outcomes after severe traumatic brain injury requiring decompressive craniectomy: a comparison of the CRASH and IMPACT prognostic models. *Injury*. <http://dx.doi.org/10.1016/j.injury.2016.04.017>.
- Horak, Z., Pokorny, D., Fulin, P., Slouf, M., Jahoda, D., Sosna, A., 2010. Polyetheretherketone (PEEK). Part I: prospects for use in orthopaedics and traumatology. *Acta Chir. Orthop. Traumatol. Cechoslov.* 77, 463–469.
- Horgan, T.J., Gilchrist, M., 2003. The creation of three-dimensional finite element models for simulating head impact biomechanics. *Int. J. Crashworthiness* 8, 353–366.
- Horgan, T.J., Gilchrist, M.D., 2004. Influence of FE model variability in predicting brain motion and intracranial pressure changes in head impact simulations. *Int. J. Crashworthiness* 9, 401–418.
- Jacquemoud, C., Bruyère-Garnier, K., Coret, M., 2007. Methodology to determine failure characteristics of planar soft tissues using a dynamic tensile test. *J. Biomech.* 40, 468–475.
- Jenkinson, M., Pechaud, M., Smith, S., 2005. BET2: MR-based estimation of brain, skull and scalp surfaces. In: *Proceedings of the Eleventh Annual Meeting of the Organization for Human Brain Mapping*.
- Jérusalem, A., Dao, M., 2012. Continuum modeling of a neuronal cell under blast loading. *Acta Biomater.* 8, 3360–3371.
- Jirousek, O., Jira, J., Jírová, J., Micka, M., 2005. Finite element model of human skull used for head injury criteria assessment. In: Gilchrist, M.D. (Ed.), *IUTAM Symposium on Impact Biomechanics: From Fundamental Insights to Applications*. Springer, Netherlands, 459–467.
- Jockisch, K.A., Brown, S.A., Bauer, T.W., Merritt, K., 1992. Biological response to chopped-carbon-fiber-reinforced peek. *J. Biomed. Mater.* 26, 133–146.
- Kang, H.S., Willinger, R., Diaw, B., Chinn, B., 1997. Validation of a 3D anatomic human head model and replication of head impact in motorcycle accident by finite element modeling. In: *Proceedings of the 41st Stapp Car Crash Conference, Lake Buena Vista, USA*, pp. 329–338.
- Khalil, T.B., Hubbard, R.P., 1977. Parametric study of head response by finite element modeling. *J. Biomech.* 10, 119–132.
- Khatam, H., Liu, Q., Ravi-Chandar, K., 2014. Dynamic tensile characterization of pig skin. *Acta Mech. Sin.* 30, 125–132.
- Kleiven, S., Hardy, W.N., 2002. Correlation of the FE model of the human head with local brain motion-consequences for injury prediction. In: *Proceedings of the 46th Stapp Car Crash Conference, Ponte Vedra, USA, Society of Automotive Engineers (SAE)*, SAE Paper No. 2002-22-0007, pp. 123–144.
- Liu, Z.S., Luo, X.Y., Lee, H.P., Lu, C., 2007. Snoring source identification and snoring noise prediction. *J. Biomech.* 40, 861–870.
- Lloyd, A.M., Nightingale, R.W., Song, Y., Luck, J.F., Cutcliffe, H., Myers, B.S., Bass, C.D., 2014. The response of the adult and ATD heads to impacts onto a rigid surface. *Accid. Anal. Prev.* 72, 219–229.
- Maracci, M., Kon, E., Zaffagnini, S., Giardino, R., Rocca, M., Corsi, A., Benvenuti, A., Bianco, P., Quarto, R., Martin, I., Muraglia, A., Cancedda, R., 1999. Reconstruction of extensive long-bone defects in sheep using porous hydroxyapatite sponges. *Calcif. Tissue Int.* 64, 83–90.
- Melvin, J.W., Robbins, D.H., Roberts, V.L., 1969. The mechanical behavior of the diploë layer of the human skull in compression. *Dev. Mech.* 5, 811–818.
- Milchenko, M., Marcus, D., 2013. Obscuring surface anatomy in volumetric imaging data. *Neuroinformatics* 11 (1), 65–75.
- Olmi, R.M., Ravaglioli, A., Krajewski, A., Pizzoferrato, A., 1984. Impianti di idrossiapatite in femori di conigli. Osservazioni istologiche e microradiografiche. *Chir. Organi Mov.* 69, pp. 383–390.
- Ommaya, A.K., Fass, F., Yarnell, P., 1968. Whiplash injury and brain damage: an experimental study. *JAMA* 204, 285–289.
- Ottenio, M., Tran, D., Annaidh, A.N., Gilchrist, M.D., Bruyère, K., 2015. Strain rate and anisotropy effects on the tensile failure characteristics of human skin. *J. Mech. Behav. Biomed. Mater.* 41, 241–250.
- Piitulainen, J.M., Kauko, T., Aitasalo, K.M.J., Vuorinen, V., Vallittu, P.K., Posti, J.P., 2015. Outcomes of cranioplasty with synthetic materials and autologous bone grafts. *World Neurosurg.* 83, 708–714.
- Posti, J.P., Piitulainen, J.M., Hupa, L., Fagerlund, S., Frantzén, J., Aitasalo, K.M.J., Vuorinen, V., Serlo, W., Syrjänen, S., Vallittu, P.K., 2016. A glass fiber-reinforced composite – bioactive glass cranioplasty implant: a case study of an early development stage implant removed due to a late infection. *J. Mech. Behav. Biomed. Mater.* 55, 191–200.
- Rae, P., Brown, E., Orler, E., 2007. The mechanical properties of poly(ether-ether-ketone) (PEEK) with emphasis on the large compressive strain response. *Polymer* 48, 598–615.
- Rashid, B., Destrade, M., Gilchrist, M.D., 2014. Mechanical characterization of brain tissue in tension at dynamic strain rates. *J. Mech. Behav. Biomed. Mater.* 33, 43–54.
- Rivard, C.H., Rhalimi, S., Coillard, C., 2002. In vivo biocompatibility testing of peek polymer for a spinal implant system: a study in rabbits. *J. Biomed. Mater.* 62, 488–498.
- Rosenthal, G., Ng, I., Moscovici, S., Lee, K., Lay, T., Martin, C., Manley, G.T., 2014. Polyetheretherketone implants for the repair of large cranial defects: a 3-center experience. *Neurosurgery* 75, 523–529.
- Ruan, J.S., Khalil, T., King, A.I., 1991. Human head dynamic response to side impact by finite element modeling. *J. Biomech. Eng.* 113, 276–283.
- Sadigh, S., Reimers, A., Andersson, R., Laflamme, L., 2004. Falls and fall-related injuries among the elderly: a survey of residential-care facilities in a Swedish municipality. *J. Community Health* 29, 129–140.
- Sahoo, D., Deck, C., Willinger, R., 2014. Development and validation of an advanced anisotropic visco-hyperelastic human brain FE model. *J. Mech. Behav. Biomed. Mater.* 33, 24–42.
- Sahoo, D., Deck, C., Yoganandan, N., Willinger, R., 2016. Development of skull fracture criterion based on real-world head trauma simulations using finite element head model. *J. Mech. Behav. Biomed. Mater.* 57, 24–41.
- Schulz, B.W., Lee, W.E., Lloyd, J.D., 2008. Estimation, simulation, and experimentation of a fall from bed. *J. Rehabil. Res. Dev.* 45, 1227–1236.
- Shuck, L.Z., Advani, S.H., 1972. Rheological response of human brain tissue in shear. *J. Basic Eng.* 94, 905–911.
- Smith, S.M., 2002. Fast robust automated brain extraction. *Human Brain Mapp.* 17 (3), 143–155.
- Smith, S.M., Jenkinson, M., Woolrich, M.W., Beckmann, C.F., Behrens, T.E.J., Johansen-Berg, H., Bannister, P.R., De Luca, M., Drobnjak, I., Flitney, D.E., Niaz, R., Saunders, J., Vickers, J., Zhang, Y., De Stefano, N., Brady, J.M., Matthews, P.M., 2004. Advances in functional and structural MR image analysis and implementation as FSL. *NeuroImage* 23 (S1), 208–219.
- Stalnaker, R.L., 1969. *Mechanical Properties of the Head* (Ph.D. dissertation). West Virginia University.
- Stefini, R., Esposito, G., Zanotti, B., Iaccarino, C., Fontanella, M.M., Servadei, F., 2013. Use of “custom made” porous hydroxyapatite implants for cranioplasty: postoperative analysis of complications in 1549 patients. *Surg. Neurol. Int.*, 4–12.
- Takhounts, E.G., Ridella, S.A., Hasija, V., Tannous, R.E., Campbell, J.Q., Malone, D., Danelson, K., Stitzel, J., Rowson, S., Duma, S., 2008. Investigation of traumatic brain injuries using the next generation of simulated injury monitor (SIMon) finite element head model. *Stapp Car Crash J.* 52, 1–31.
- Takhounts, E., Eppinger, R., 2003. On the development of the SIMon finite element head model. In: *Proceedings of the 47th Stapp Car Crash Conference, San Diego, USA, Society of Automotive Engineers (SAE)*, pp. 107–133.
- Tong, P., Fung, Y.C., 1976. The stress-strain relationships for the skin. *J. Biomech.* 9, 649–657.
- Tse, K.M., Tan, L.B., Lee, S.J., Lim, S.P., Lee, H.P., 2015. Investigation of the relationship between facial injuries and traumatic brain injuries using a realistic subject-specific finite element head model. *Accid. Anal. Prev.* 79, 13–32.
- Ueno, K., Melvin, J.W., Lundquist, E., Lee, M.C., 1989. Two-dimensional finite element analysis of human brain impact responses: application of a scaling law. *Crashworthiness and Occupant Protection in Transportation Systems*, New York, ASME, AMD, vol. 106.
- Van Essen, D.C., Smith, S.M., Barch, D.M., Behrens, T.E., Yacoub, E., Ugurbil, K., 2013. The Wu-Minn human connectome project: an overview. *Neuroimage* 80, 62–79.
- Vogel, H.G., 1972. Influence of age, treatment with corticosteroids and strain rate on mechanical properties of rat skin. *Biochim. Biophys. Acta* 286, 79–83.
- Ward, C.C., Chan, M., Nahum, A.M., 1980. Intracranial pressure – a brain injury criterion. In: *Proceedings of the 24th Stapp Car Crash Conference, Warrendale, USA, Society of Automotive Engineers (SAE)*, SAE Paper No. 801304, pp. 347–360.
- Willinger, R., Taleb, L., Kopp, C.M., 1995. Modal and temporal analysis of head mathematical models. *J. Neurotrauma* 12, N4.
- Willinger, R., Kang, H.S., Diaw, B.M., 1999. 3D human head finite element model validation against two experimental impacts. *Ann. Biomed. Eng.* 27, 403–410.
- Willinger, R., Baumgartner, D., Chinn, B., Neale, M., 2000. Head tolerance limits derived from numerical replication of real world accidents. In: *Proceedings of the International ICORBI Conference on the Biomechanics of Impacts, Montpellier, France*, pp. 209–221.
- Wood, J.L., 1971. Dynamic response of human cranial bone. *J. Biomech.* 4, 1–12.
- Zahouani, H., Paillet-Mattei, C., Sohm, B., Vargiolu, R., Cenizo, V., Debret, R., 2009. Characterization of the mechanical properties of a dermal equivalent compared with human skin in vivo by indentation and static friction tests. *Skin Res. Technol.* 15, 68–76.
- Zahr Viñuela, J., Pérez-Castellanos, J.L., 2015. The anisotropic criterion of von Mises (1928) as a yield condition for PMMCs. A calibration procedure based on numerical cell-analysis. *Compos. Struct.* 134, 613–632.
- Zhang, L., Yang, K.H., Dwarampudi, R., Omori, K., Li, T., Chang, K., Hardy, W.N., Khalil, T.B., King, A., 2001. Recent advances in brain injury research: a new human head model development and validation. In: *Proceedings of the 45th Stapp Car Crash Conference, San Antonio, USA, Society of Automotive Engineers (SAE)*, SAE Paper No. 2001-22-0017, pp. 369–394.
- Zhou, Z., Jiang, B., Cao, L., Zhu, F., Mao, H., Yang, K.H., 2016. Numerical simulations of the 10-year-old head response in drop impacts and compression tests. *Comput. Methods Prog. Biomed.* 131, 13–25.
- Zhou, C., Khalil, C.T.B., King, A.I., 1995. A new model comparing impact responses of the homogeneous and inhomogeneous human brain. In: *Proceedings of the 39th Stapp Car Crash Conference, San Diego, USA, Society of Automotive Engineers (SAE)*, SAE Paper No. 952714, pp. 121–137.